www.vbripress.com, www.amlett.com, DOI: 10.5185/amlett.2011.5261 Published online by the VBRI press in 2012

Thickness uniformity and microstructure of disc shape spray formed Al-Si-Pb alloys

Rashmi Mittal, Aruna Tomar, Devendra Singh*

Department of Metallurgical and Materials Engineering, Indian Institute of Technology, Roorkee 247667, India

*Corresponding author. Fax: (+91) 1332 273560, 285243; E-mail: dev27fmt@iitr.ernet.in

Received: 30 May 2011, Revised: 22 Aug 2011 and Accepted: 26 Aug 2011

ABSTRACT

Spray forming technique was employed to produce a near net-shape disc of Al-Si-Pb alloys. Different substrate distances and inclination angles were studied to obtain the disc shape preforms. The substrate was also offset by 40 mm from the atomizer axis in case of 15 and 30 degree inclination angles. Microstructures were investigated in different regions of the preforms. Results exhibited equiaxed grains of primary Al and Si was present within these grains and along the grain boundary. The size of the Al grains was 20-30 μm and size of Si particles was sub-micron to 5 μm. The size of Pb particles varied from sub-micron to 20 μm and it was uniformly dispersed throughout the aluminum phase. Copyright © 2011 VBRI press.

Keywords: Disc shape performs; microstructure; spray forming; aluminum alloys.

Rashmi Mittal obtained her B.Sc. and M.Sc. from kurukshetra university, yanunanagar, India. At present she is pursuing Ph.D. in "Spray Forming" field, from department of Metallurgical and materials engineering, IIT Roorkee, India. Her main research interests are advanced materials and modeling.

Aruna Tomar obtained her B.Sc. and M.Sc. from C.C.S. university, Meerut, India. She did her Ph.D. in "Spray Forming", from department of Metallurgical and materials engineering, IIT Roorkee, India. Her main research interests are advanced materials and modeling.

Devendra Singh is presently working as an assistant professor in the department of metallurgical and materials engineering, IIT Roorkee, India. He did his B. Tech, M. Tech and Ph.D. in Metallurgical engineering from IIT Kanpur. His present areas of research are Spray Forming, Modeling, Thin films and gas dynamics.

Introduction

Aluminum based alloys have the advantage of high strength to weight ratio, and therefore they are widely used in the automotive and aerospace industries. The liquid immiscible alloys based on Al–Pb system are potential materials for bearing alloys [**1–17**] because they possess superior performance like superior friction properties, low cost of production, high thermal conductivity and high corrosion resistance than other aluminum bearing alloys [**3, 9, 10, 17**]. Processing of Al–Pb alloys by the conventional casting [**18**] techniques is difficult due to liquid immiscibility in a wide range of temperature and composition; and also large density difference of the constituent phases compared to Al alloys [**1, 7, 9**]. In the past, several techniques, different from conventional casting, have been employed to prevent segregation of lead during melt solidification. Techniques based on powder metallurgy [**2**], stir casting [**1, 14**], rheocasting [**9**], melt spinning [**12**], strip casting [**19**] and spray forming [**14–16**], results in a uniform distribution of lead particles in Al matrix. Among these techniques, spray forming possesses several advantages in effective microstructural control together with producing a near net shape preform in a less number of processing steps [**14–16**].

During spray atomization and subsequent deposition a detailed study of the solidification mechanisms that govern the evolution of microstructure is very complex due to the extreme differences in thermal environment both before and after impact of the droplets with the deposition surface. During spray atomization, the violent and rapid extraction of thermal energy by the atomization gas promotes the formation of highly refined grain structures [**17**]. In

contrast, during subsequent deposition the solidification conditions are governed by relatively slow cooling rates [**11, 20**]. The microstructure of spray-atomized and deposited materials is generally reported to exhibit spheroidal or "equiaxed" grains [**21**], a feature that is consistently observed regardless of alloy composition [**22, 23**].

Various shapes like disc [**24, 25**], billet [**26, 27-30**], tube [**26**] and ring [**31**] can be produced by this process. The disintegrated or atomized droplets during the process follow a particular distribution [**31, 32**] and therefore some special arrangements are required to produce aforementioned shapes of desired dimensions. In the present work Al-Si-Pb alloys were spray formed in the form of a disc and then their characteristics such as thickness uniformity of the disc and microstructure were investigated.

Experimental

A Schematic of spray forming set-up is given elsewhere [**33**]. The alloy was allowed to melt into a graphite crucible placed inside an induction furnace. At centre of the bottom of crucible an exchangeable graphite melt delivery tube was fitted to produce melt flow stream. A stopper road was used to either open or close the entrance of the delivery tube. Other end of delivery tube was fitted into the atomizer which was placed above the cooling chamber. Height of cooling chamber was 1500 mm. The stopper rod was raised up after the starting of gas flow in atomizer to start the atomization of melt and thereby spray deposition. Vertically falling liquid metal stream was interacted with high energy gas jet at the tip of melt delivery tube which promote atomization of melt into spray of small size droplets. This atomization was performed inside the cooling or spray chamber and atomized droplets were deposited over a copper substrate, placed at a variable distance from the atomizer. Copper substrate could be inclined at desired angle from the horizontal axis and also could be rotated at varying rpm to get a disc shape of preform.

The base alloy used in the present work consisted of Al-Si. This alloy was superheated to 200^0C above its melting temperature in the graphite crucible using the induction furnace. Different amount (0, 10, 15, 20, 25 wt. %) of lead was added in the Al-Si alloy before atomization of melt. In each run 800 gm of Al-Si-Pb alloy was charged in crucible. Nitrogen gas was supplied for atomization prior to melt flow. The atomization was carried out at a N_2 gas pressure of 10 bar. The spray droplets were deposited over a rotating (240 rpm) copper substrate (diameter 200 mm) centered along the axis of the atomizer, which was either inclined to 0^o, 15^o and 30^o or/and offset at a distance of 40 mm from the central axis of the atomizer to achieve a disc shape preform. These preforms were taken out of the substrate after deposition. Thickness uniformity of the disc shape preforms was observed under different process parameters.

Samples from the central and peripheral regions of the preform (as shown in **Fig. 1** with their locations) were cut down for its microstructural study. These samples were polished using standard metallographic technique of polishing with an emery paper of 1/0, 2/0, 3/0 and 4/0 specification and then followed by wheel cloth polishing using an emulsion of alumina powder particles suspended in water. Afterwards these samples were polished by kerosene oil and brasso. Then samples were etched with Keller's reagent and examined with Letiz optical microscope (OM) and JEOL JXA840A scanning electron microscope (SEM). Scanning electron microscope was operated at an accelerating voltage of 20-25 KV.

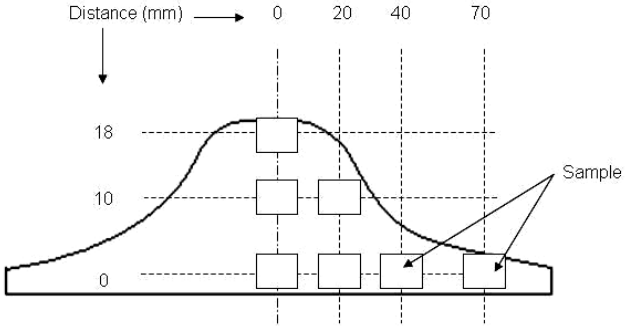

Fig. 1. Locations of samples cut from spray deposit for microstuctural study.

Results and discussion

Thickness uniformity of disc shape preform

The side view of the deposit produced at three different distances and three different inclination angles are shown in **Fig. 2**. The substrate was also offset by 40 mm from the atomizer axis in case of 15 and 30^0 inclination angles. This figure shows the thickness uniformity of the deposit for the different combinations and values of parameters. It can be seen that the thickness uniformity of the deposit produced at an angle of 30^0 with an offset distance of 40 mm (**Fig. 2 d**) is higher than that of at 0^0 (**Fig. 2 b**).

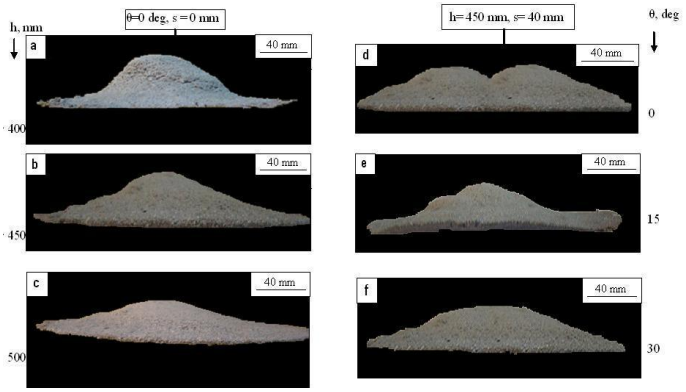

Fig. 2. Shape of spray deposit produced at different substrate distances (h), offset distances (s) and inclination angles (θ): (a) h= 400, θ = 0, s=0; (b) h = 450, θ = 0, s=0; (c) h = 500, θ = 0, s=0; (d) h = 450, θ = 0, s=40; (e) h = 450, θ = 15, s=40 and (f) h=450 mm, θ = 30 deg , s=40 mm.

In other words, the thickness uniformity of the deposit increases with the increase in inclination angle with offset distance of the substrate from atomizer axis. However, the loss of deposited particles increases with the increase in inclination angle for the same size of the substrate which is obvious from the geometry with the consideration of conical shape of the spray cone. The thickness uniformity also increases with the increase in deposition distance from

atomizer as observed from **Fig. 2** (**a-c**). However, the loss of deposited particles also increases with the increase in deposition distance for the same size of preform which is also obvious from the geometry.

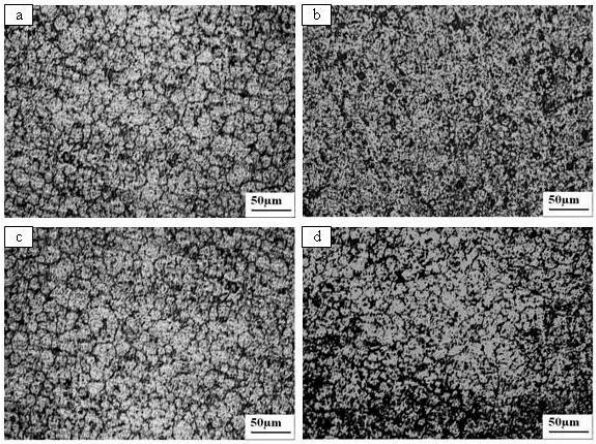

Fig. 3. Optical micrographs of spray deposited Al-6Si alloy showing (a) top; (b) middle; (c) bottom and (d) peripheral regions.

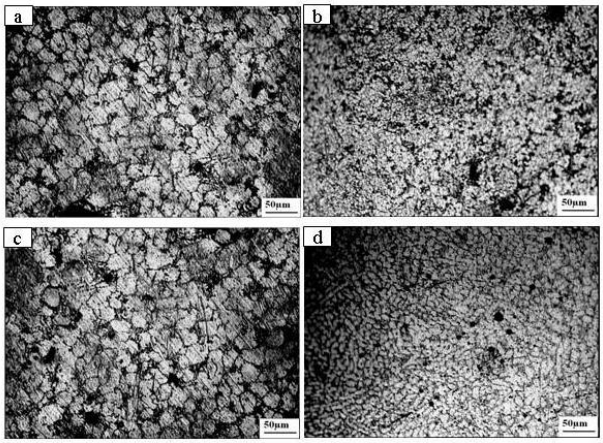

Fig. 4. Optical micrographs of spray deposited Al-6Si-10Pb alloy showing distribution of Pb and Si particles at (a) top; (b) middle; (c) bottom and (d) peripheral regions.

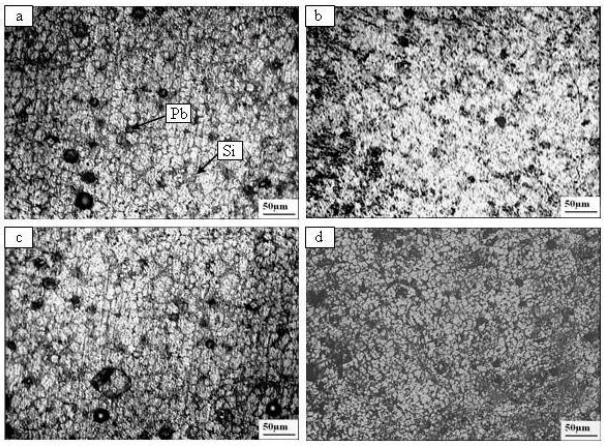

Fig. 5. Optical micrographs of spray deposited Al-6Si-15Pb alloy showing distribution of Pb and Si particles at (a) top; (b) middle; (c) bottom and (d) peripheral regions.

Microstructure

Optical micrographs taken at four different locations of the deposit viz. (a) top, (b) middle, (c) bottom and (d) peripheral regions are shown from **Fig. 3-7** for different Pb contents varying from 0 to 25%.

Fig. 3 shows microstructure of spray formed Al-Si alloy (i.e. no lead). Equiaxed grains of primary Al were observed and Si was present within these grains and along the grain boundary. Dark gray colour in microstructure represents Si phase. The size of the Al grains was 20-30 μm and size of Si particles was sub-micron to 5 μm.

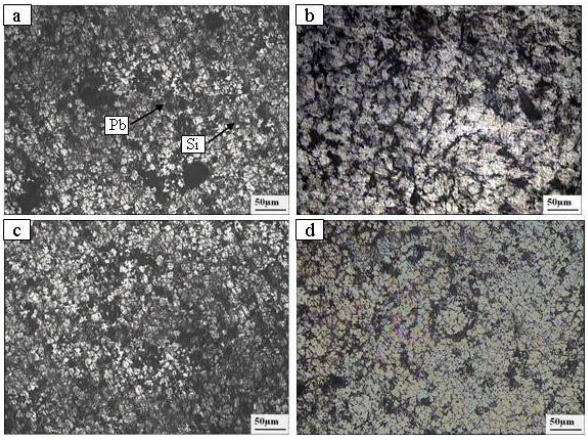

Fig. 6. Optical micrographs of spray deposited Al-6Si-20Pb alloy showing distribution of Pb and Si particles at (a) top; (b) middle; (c) bottom and (d) peripheral regions.

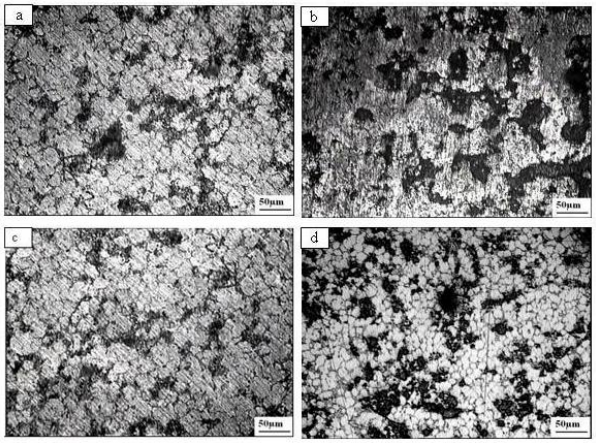

Fig. 7. Optical micrographs of spray deposited Al-6Si-25Pb alloy showing distribution of Pb and Si particles at (a) top; (b) middle; (c) bottom and (d) peripheral regions.

Dark black colour represents the Pb phase in **Fig. 4-7**. It can be seen that the Pb distribution is almost uniform throughout the aluminum phase. The size of Pb particles varies from sub-micron to 10 μm at central regions i.e. top, middle and bottom, sub-micron to 5 μm at peripheral region in case of 10% Pb. Similarly, the lead particles size varies from sub-micron to 15, sub-micron to 20 and sub-micron to 25 μm at central (top, middle and bottom) regions and sub-micron to 10, sub-micron to 15 and sub-micron to 20 μm at peripheral region in case of 15, 20, and 25% Pb, respectively. It can also be seen that the size of the aluminum grains is almost same at the bottom and top

regions whereas it is lower at peripheral region. In middle region the grain size is a little bit coarser than at the top or bottom region. The aluminum grain size at central regions i.e. top, middle and bottom is 5-35 μm and it is 2-20 μm at peripheral region for all values of the lead content.

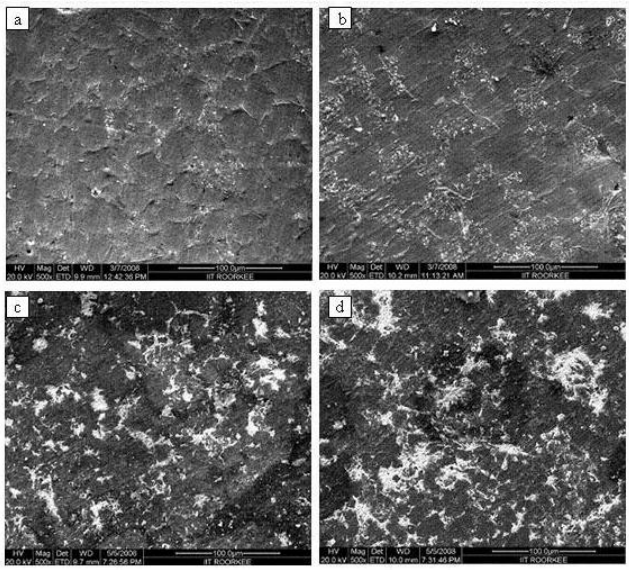

Fig. 8. SEM micrographs showing the Pb (white phase) distribution in Al-6Si matrix for (a) 10; (b) 15; (c) 20 and (d) 25 % Pb.

Fig. 8 shows the SEM micrographs for (**a**) 10, (**b**) 15, (**c**) 20 and (**d**) 25% Pb at central region of the deposit. It can be seen that grain boundaries are not as clear as in optical micrographs as percentage of lead increases from 10 to 25%. The white phase is Pb, which is distributed along grain boundaries and inside the Al grains. Maximum amount of lead is on the grain boundaries. Pb particles size varies from sub-micron to 25 μm and it is higher for higher lead content.

Theory of thickness uniformity of disc shape perform

Mass flux of the droplets varies from centre to periphery of the spray cone and hence the spray deposit or preform can not have a uniform thickness. The variation in preform thickness needs to be determined before further study of its properties because it will affect them and hence their studies without reporting the thickness variation of the deposit can produce misleading results. In present study inclination angle, offset distance and distance of substrate from the atomizer were observed to affect the thickness variation or uniformity of the spray deposit which can be explained as follows.

Effect of inclination angle

At 0^0 inclination angle of the substrate from horizontal plane and without its offsetting, the deposition or substrate area per unit change in radius of the substrate increases with the increase in radius of the substrate i.e.
If

$$A_s = \pi r_s^2 \qquad (1)$$

Then,

$$\frac{dA_s}{dr_s} = 2\pi r_s \qquad (2)$$

Therefore, the mass distribution of particles/ droplets in spray cone should also increase in same proportion to get a deposit of uniform thickness. But, unfortunately this mass decreases instead of increasing as given by the following Gaussian distribution [**31, 32**] function.

$$\dot{m} = \dot{m}_{\max} \exp\left(-a\, r^K\right) \qquad (3)$$

Where, $\dot{m}_{\max}$ is the maximum mass flux in the spray cone, K (=1.4) is a constant and a is a radial distribution coefficient given by

$$a = \ln 2\left(\frac{1}{r_{0.50}}\right)^K \qquad (4)$$

Where, $r_{0.5}$ is the half width of the spray cone.
From Equations (3) and (4)

$$\dot{m} = \dot{m}_{\max} \exp\left[-\ln 2\left(\frac{r}{r_{0.50}}\right)^K\right] \qquad (5)$$

Therefore, at 0^0 inclination angle it is impossible to produce a deposit of uniform thickness. At an inclination angle `θ` of the substrate the $\dot{m}_{\max}$ will shift continuously towards periphery of the deposit with the increase in its thickness i.e. more mass is shifted towards periphery and hence inclination of the substrate increases the thickness uniformity of the deposit.

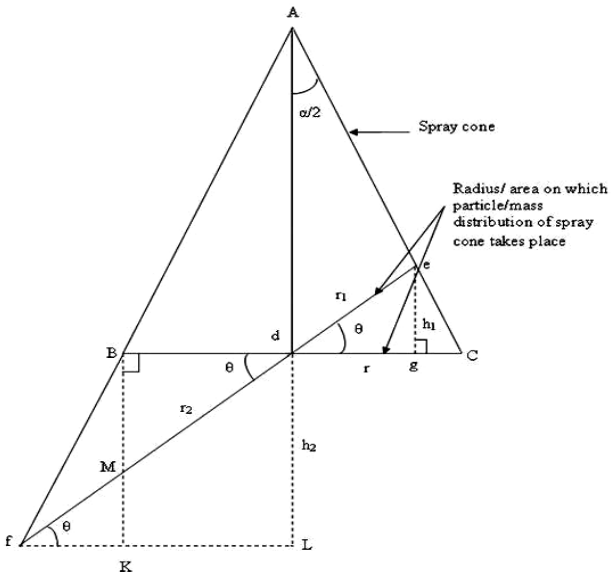

Fig. 9. Schematic to show the radius/area on which particle/mass distribution of spray cone takes place after tilting substrate an angle 'θ'.

The thickness uniformity with the increase in inclination angle will also increase due to the distribution of same mass

of particles over more area of the inclined surface in the same spray cone as shown in **Fig. 9**. Mathematically, the mass distribution of the spray cone along the tilted substrate can be given by the Equation (5) in a modified form as explained below.

The radius of depositing mass will be distributed from r_1 to r_2 on the substrate surface and hence mass distribution will also vary from $\dot{m}_1$ *to* $\dot{m}_2$ given by the following equations:

$$\dot{m}_1 = \dot{m}_{\max} \exp\left[-\ln 2 \left(\frac{r_1}{r_{0.50}} \right)^K \right] \quad (6)$$

and

$$\dot{m}_2 = \dot{m}_{\max} \exp\left[-\ln 2 \left(\frac{r_2}{r_{0.50}} \right)^K \right] \quad (7)$$

where r_1 and r_2 are given by following expressions

$$r_1 = \frac{r}{\cos\theta + \sin\theta \tan\alpha/2} \quad (8)$$

and

$$r_2 = \frac{r}{\cos\theta - \sin\theta \tan\alpha/2} \quad (9)$$

with every rotation of substrate, the mass deposition rate on every point of substrate will vary from $\dot{m}_1$ *to* $\dot{m}_2$. So, effective or average deposition on every point of substrate is given by the following equation.

$$\dot{m}_\theta = \frac{\dot{m}_1 + \dot{m}_2}{2} = \frac{\dot{m}_{\max}}{2} \left[\exp\left(-\ln 2 \left(\frac{r_1}{r_{0.50}} \right)^K \right) + \exp\left(-\ln 2 \left(\frac{r_2}{r_{0.50}} \right)^K \right) \right] \quad (10)$$

Fig. 10 shows a plot between the ratio of mass deposition rate at inclination angle of 30^0 ($\dot{m}_{30}$) to that of at 0^0 ($\dot{m}_0$) and the ratio of spray cone radius (r) to half width of spray cone ($r_{0.50}$) for a spray cone angle of 40^0. It can be seen that the mass in spray cone first decreases from centre to periphery and then it increases, which is required to increase the thickness uniformity. Therefore, the thickness uniformity was observed to increase in **fig. 2** (**d-f**) with the increase in inclination angle from 0 to 30^0.

Effect of offset distance

The offsetting of substrate after its tilting can be in left or right side of the central axis (or atomizer axis) of the spray cone. Both the offsetting will have different effect on mass distribution of spray cone over the substrate surface. In present study substrate was tilted anti-clockwise and moved in the right side. To understand the effect of offsetting on thickness uniformity of the deposit, no tilting is assumed for the simplicity. Therefore, for horizontal substrate with an offset distance 's' as shown in **fig. 11**, the mass distribution of droplets in spray cone on the substrate in left and right of its centre can be given by the following equations which are derived from equation (5).

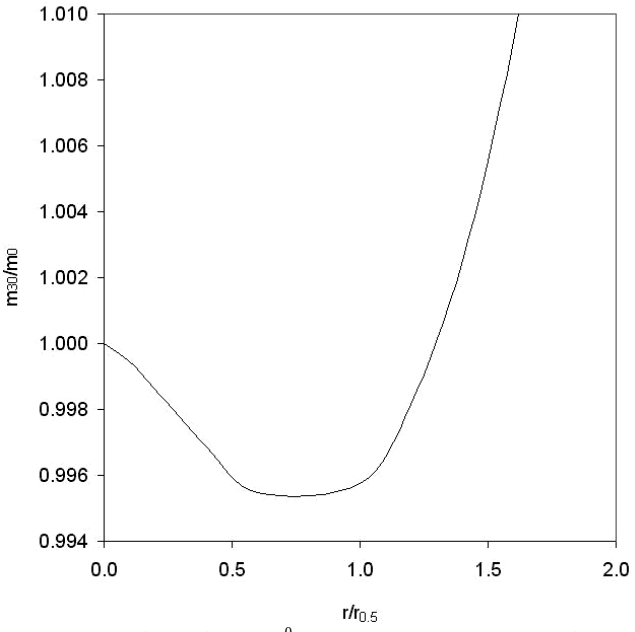

Fig. 10. Ratio of mass flux at 30^0 inclination angle (m_{30}) to mass flux rate at 0^0 angle (m_0) with ratio of radius $r/r_{0.5}$ of the spray cone.

In right hand side the equation is

$$\dot{m}_3 = \dot{m}_{\max} \exp\left[-\ln 2 \left(\frac{r+s}{r_{0.50}} \right)^K \right] \quad (11)$$

and in left hand side the equations are

$$\dot{m}_4 = \dot{m}_{\max} \exp\left[-\ln 2 \left(\frac{s-r}{r_{0.50}} \right)^K \right] \quad \text{for } 0 \le r \le s \quad (12)$$

$$\dot{m}_5 = \dot{m}_{\max} \exp\left[-\ln 2 \left(\frac{r-s}{r_{0.50}} \right)^K \right] \quad \text{for } r \ge s \quad (13)$$

With every rotation of substrate, the mass deposition rate on every point of substrate will vary from $\dot{m}_3$ *to* $\dot{m}_4$ for $0 \le r \le s$ and $\dot{m}_3$ *to* $\dot{m}_5$ for $r \ge s$. Therefore, there will be two regions on the substrate having mass deposition given by the following equations.

$$\dot{m}_{s1} = \frac{\dot{m}_3 + \dot{m}_4}{2} = \frac{\dot{m}_{\max}}{2} \left[\exp\left(-\ln 2 \left(\frac{r+s}{r_{0.50}} \right)^K \right) + \exp\left(-\ln 2 \left(\frac{s-r}{r_{0.50}} \right)^K \right) \right]$$

for $0 \le r \le s$ (14)

and

$$\dot{m}_{s2} = \frac{\dot{m}_3 + \dot{m}_5}{2} = \frac{\dot{m}_{max}}{2}\left[\exp\left(-\ln 2\left(\frac{r+s}{r_{0.50}}\right)^K\right) + \exp\left(-\ln 2\left(\frac{r-s}{r_{0.50}}\right)^K\right)\right]$$

for $r \geq s$ (15)

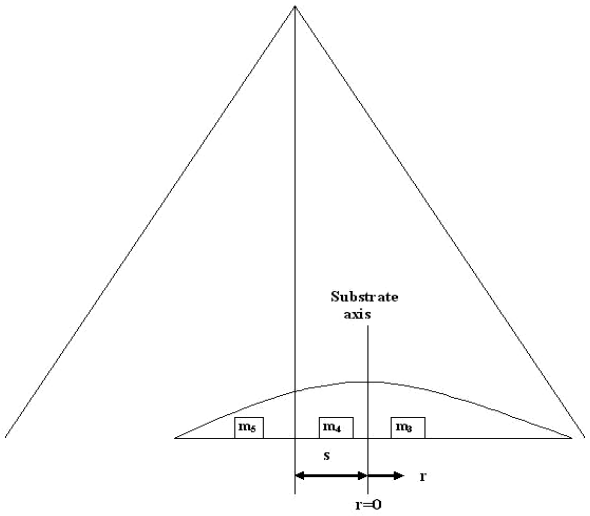

Fig. 11. Schematic to represent the mass distribution about substrate axis with an offset distance 's' from spray cone axis.

Fig. 12 shows a plot between the ratio of mass deposition rate at an offset distance of 40 mm ($\dot{m}_{40}$) to that of maximum mass flux and the ratio of spray cone radius (r) to half width of spray cone ($r_{0.50}$). It can be seen that the mass on substrate in the spray cone first decreases up to 's' from cone centre to periphery and then it increases as compared to that of without offsetting, which is required to increases the thickness uniformity. Therefore, by offsetting the substrate from 0 to 40 mm a more uniform deposit in thickness was produced as shown by comparing the deposit shape in **fig. 2** (**b**) and (**d**). In **fig. 12** it can also be seen that the shape generated theoretically from the above explained model is similar to that produced experimentally in **fig. 2** (**d**).

Effect of substrate distance

Mass flux distribution in spray cone is given by [**25**] the following equation

$$\dot{m}(r,h) = \dot{m}_{\max_o}\left(\frac{h_0}{h}\right)^2 \exp\left[-a_0\left(\frac{h_0}{h}\right)^K .r^K\right] \qquad (16)$$

Where, $\dot{m}_{\max_0}$ is the maximum mass flux in spray cone at distance h_0 and a_0 is the radial distribution coefficient at distance h_0, which is given by

$$a_0 = \ln 2\left(\frac{1}{r_{0.50}}\right)^K \qquad (17)$$

From Equations (16) and (17) for K=1.4 the following equation can be obtained.

$$\frac{\dot{m}(r,h)}{\dot{m}_{\max_0}} = \left(\frac{h_0}{h}\right)^2 \exp\left[-0.693\left(\frac{r}{r_{0.50}}.\frac{h_0}{h}\right)^{1.4}\right] \qquad (18)$$

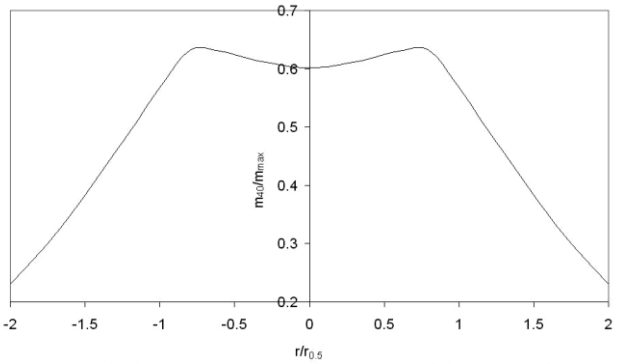

Fig. 12. Variation of mass distribution in spray cone on the substrate with an offset distance of 40 mm

A plot of above Equation (18) in terms of dimensionless terms $\dot{m}(r,h)/\dot{m}_{\max_o}$ versus $r/r_{0.50}$ for different values of h / h_0 is shown in **Fig. 13**. It can be seen that the mass flux distribution ($\dot{m}$) uniformity with spray radius (r) increases with the increase in spray distance (h). This increase in thickness uniformity was observed in present study as shown in **Fig. 2** (**a-c**) with the increase in substrate distance from 400 to 500 mm. It has been observed that both tilting as well as offsetting of the substrate increases the thickness uniformity of the preform. Therefore, combination of both tilting and offsetting will give more uniform thickness of preform as observed in **Fig. 2 (f)**

Solidification & microstructure evolution

Atomized droplets in liquid, semi-solid and fully solid state deposit over the substrate kept at a distance of 450 mm. At this distance the maximum velocity of gas is about 50 m/s [**34**]. This velocity is not supposed to disintegrate further the droplets [**35**] or melt depositing on the substrate. However, the impact of the momentum of droplets striking the deposit can further break some melts on the deposit. The impact of this momentum also leads breaking of semi-solid droplets into finer fragments on the deposition surface. These fine fragments act as nuclei for the solidification of melt on the surface [**24**].

A semi-solid or semi-liquid mass is continuously depositing and solidifying on the deposition surface. This continuously depositing mass will release heat rapidly to the surroundings having high gas velocity, and already / previously deposited mass. The high gas velocity leads to high rate of heat transfer by convection and previously deposited mass leads to heat transfer by conduction from the depositing mass. Therefore, the formation of nuclei and high rate of heat transfer from the melt leads to very high solidification rate of the spray deposit and thereby formation of equiaxed structure **(fig. 3-7)**. The silicon in the structure is in particulate form, contrary to that of the convectional cast structure [**36, 37, 38**]. It also indicates rapid solidification of the deposit [**36**].

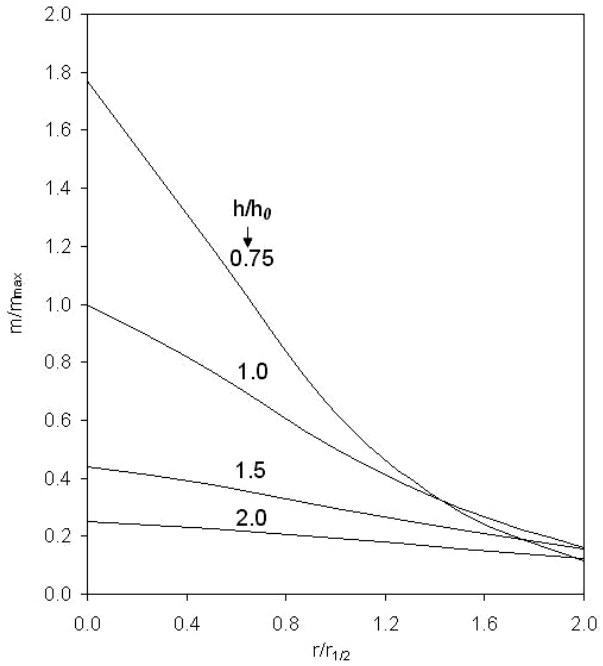

Fig. 13. Variation of spray cone mass with spray cone radius for different values of deposition distance

Molten lead will diffuse towards the liquid present in the deposit during solidification of the Al-rich deposit. Therefore, it diffuses towards the grain boundary of aluminum and accumulates over there in small droplets (**Fig. 8**). More amount of lead in aluminum rich melt means more accumulation of lead at the grain boundaries (**Fig. 4-8)**. The shape of these lead droplets will depend on their spherodization time and the solidification time of Al-rich melt. If Al-rich melt solidify after the spherodization time of lead, the lead droplet will be spherical **(Fig. 4-5** and **8 (a-b)** otherwise non-spherical **(Fig. 6-7** and **8 (c-d)**. The large size lead droplets will take more time to spherodize and hence these will remain non spherical. It was revealed in both optical and SEM micrographs.

Silicon will also diffuse to the grain boundary and solidify before solidification of the lead. Therefore, some silicon particles at grain boundaries were observed to be surrounded by lead.

The microstructure of the deposit was found to depend on the central and peripheral regions of the deposit **(Fig. 3-7)**. The small thickness of the deposit at peripheral region leads to an increase in the heat transfer rate ($\dot{Q}$ α dT/dx) by conduction and hence more cooling rate at peripheral region as compared to that of the central region. The more cooling rate at peripheral region leads to the formation of more fine grains structure as compared to that of the central region.

Heat transfer from the deposit also takes place by convection in high gas velocity field. The difference in gas velocity at the centre and periphery is not very large [**34**]. So, there will not be a significant difference in cooling rate by convection at the centre and periphery of the deposit.

No significant change in microstructure was observed at the bottom and top of the deposit, which indicate almost same solidification rate at these locations. Actually, the solidification rate cannot vary along the thickness of the deposit under steady state condition i.e. when there is no change in substrate temperature with time and metal is depositing continuously on it. It can be understood as follows. A constant mass flow rate of droplets/ particles varying in radial direction in the spray cone moves towards the substrate. The deposit grows in thickness direction with a constant rate. This deposition rate varies only in radial direction of the deposit which results in a non-uniform thickness of the deposit. It implies that the solidification rate should be constant in thickness direction and vary in radial direction. If solidification rate is not constant in thickness direction i.e. it is decreasing or increasing with the thickness, in that case one condition will arrive at which nothing or everything will solidify on top surface of the deposit. Both of these events are not occurring. Therefore, under steady state condition, solidification rate will not vary along the thickness of the deposit.

In the beginning, the substrate is at room temperature, and its temperature increases with the increases in deposit mass. So, in the beginning there is no steady state and hence up to the deposition thickness at which steady state is achieved, the solidification rate will vary. It will decrease with the increase in the deposit thickness up to the steady state condition. So, the grain size of bottom mass of the deposit should be finer to that of the top mass. But, it was not the case. It indicates same solidification rate at both the locations. Actually, the deposition stop after some time and solidification of the top surface also takes place under unsteady state condition (like bottom surface) in the high gas velocity. So, it can give rise to same solidification rate and hence same grain size.

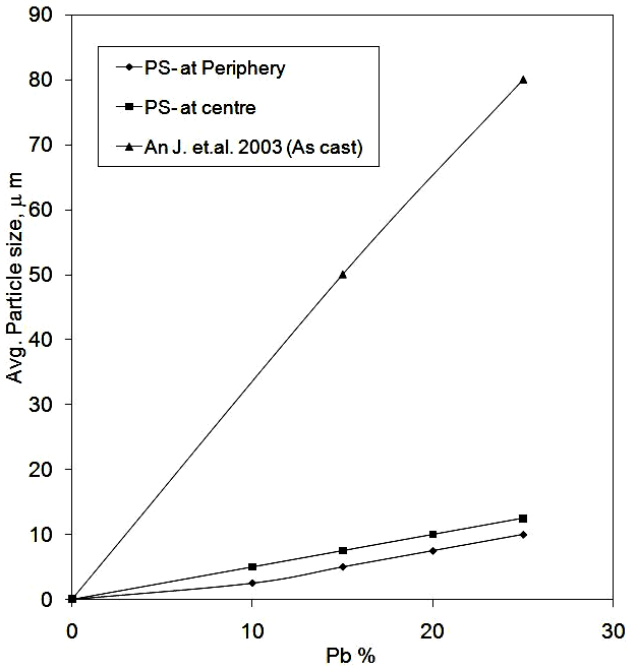

Fig. 14. Average lead particle size as a function of lead content in Al-Si-Pb alloy.

Fig. 14 shows the average lead particle size as a function of lead content in the Al-Si-Pb alloy. The values of lead particles size reported by An J. et al. [**2**] for the cast Al-Si-Pb alloy are also shown in the same figure. It can be

seen that their values and the data of the present study represent a straight line variation and the lead particle size increases with the increase in lead content. The aluminum grains are coarser in the cast alloy. In present study the size of aluminum grains is also higher at the centre as compared to that of the periphery of the deposit. Therefore, same figure also shows that the lead particles size increases with the increase in the size of aluminum grains.

Conclusion

The thickness uniformity of the disc shape deposit increases with the increase in its distance from the atomizer, with the offset distance from the atomizer axis and with the increase in its inclination angle. Lead is found uniformly dispersed in the spray deposit. The size of lead particles increases linearly with the increase in lead content and are larger at the centre as compared to that of periphery of the deposit. The size of the aluminum grains is almost same at the bottom and top regions whereas it is smaller at the peripheral region of the perform. In middle region the grain size is a little bit coarser than that of the top or bottom region. The grain boundaries are not very clear with the increase in lead content and the maximum amount of lead is distributed along the grain boundaries. Some silicon particles are observed to be surrounded by lead at the grain boundary of aluminum phase.

Reference

1. An, J.; Liu, Y.B.; Lu, Y. *Mater. Sci. Eng.* **2004**, *A 373*, 294. **DOI:** 10.1016/j.msea.2004.01.051
2. An, J.; Liu, Y.B.; Lu, Y.; Zhang, Q.Y.; Dong, C. *Wear* **2004**, *256*, 374. **DOI:** 10.1016/S0043-1648(03)00461-70
3. Ogita, Y.; Ido, Y.; Sakamoto, M. *MPR* **1991**, *46*, 37. **DOI**:10.1016/0026-0657(91)90453-8
4. Pathak, J.P.; Tiwari, S.N.; Malhotra, S.L. *Wear* **1986**, *112*, 341.
5. Pathak, J.P.; Torabian, H.; Tiwari, S.N. *Wear* **1997**, *202*, 134. **PII:** S0043-1648(96)07241-9
6. Sharma, A.; Rajan, T.V. *Wear* **1996**, *197*, 105. **DOI**: 10.1016/0043-1648(95)06861-9
7. Sharma, A.; Rajan, T.V. *Wear* **1994,** *174*, 217. **SSDI:** 0043-~648(93)06404-R)
8. Zhu, M.; Gao, Y.; Chung, C.Y.; Che, Z.X.; Luo, K.C.; Li, B.L. *Wear* **2000,** *242*, 47. **DOI:** 10.1016/S0043-1648(00)00397-5
9. Fang, X.; Fan, Z. *Scripta. Mater*. **2006,** *54*, 789. **DOI:** 10.1016/j.scriptamat.2005.11.021
10. Mohan, S.; Agarwala, V.; Ray, S. *Wear* **1992,** *157*, 9. **DOI**: 10.1016/0043-1648(92)90184-A
11. Rudrakshi, G.B.; Srivastava, V.C.; Pathak, J.P.; Ojha, S.N. *Mater. Sci. Eng.* **2004,** *A 383*, 30. **DOI:** 10.1016/j.msea.2004.02.033
12. Zhao, J.Z.; Drees, S.; Ratke, L. *Mater. Sci. Eng*. **2000,** *A 282*, 262. **PII:** S0921-5093(99)00755-8
13. Mohan, S.; Pathak, J.P.; Sarkar, S.; Chander, N. *J. Reinf. Plast. Comp*. **2007,** *11*, 37.
14. Mohan, S.; Agarwala, V.; Ray, S. *Wear* **1990,** *140*, 83. **DOI** :10.1016/0043-1648(90)90123-R
15. Mohan, S.; Agarwala, V.; Ray, S. *Mater. Sci. Eng*. **1991,** *A 144*, 215. **DOI**:10.1016/0921-5093(91)90227-E
16. Guang, R.; Jing-En, Z.; Shengqi, Xi.; Pengliang, Li. *J. Alloy Compd*. **2006,** *419*, 66. **DOI:** 10.1016/j jallcom.2005.09.057
17. Yu, F.; Dwarakadasa, D.S.; Ranganathan, S. *J. Mater. Process. Technol*. **2003,** *137*, 164. **PII:** S0924-0136(02)01085-3
18. Zhongjun, W.; Jing, Z.; Zhaojing, W.; Baohua, K. *Adv. Mat. Lett.* **2011**, *2(2)*, 153. **DOI:** 10.5185/amlett.2010.12222
19. Zhao, J. Z.; Drees, S.; Ratke, L. *Mater. Sci. Eng.* **2000,** *A282*, 262. **PII:** S0921-5093(99)00755-8
20. Shukla, P.; Mishra, N.S.; Ojha, S.N. *ASM J. Therm. Spray. Tech.* **2003,** *12*, 95. **DOI:** 10.1361/105996303770348546
21. Zhongjun, W.; Zhaojing, W.; Jing, Z. *Adv. Mat. Lett*. **2011**, ***2(2)***, 113. **(DOI:** 10.5185/amlett.2010.12217)
22. Liang, X.; Lavernia, E.J. *Mater. Sci. Eng.* **1993,** *A 161*, 221. **DOI:** 10.1016/0921-5093(93)90517-I
23. Liang, X.; Earthman, J.C.; Lavernia, E.J. *Acta metal. Mater*. **1992,** *40*, 3003.
24. Ojha, K.V.; Tomar, A.; Singh, D.; Kaushal, G.C. *Mat. Sci. Engg*. **2008,** *A 487*, 591. **DOI:** 10.1016/j.msea.2007.10.032
25. Srivastava, A.K.; Anandani, R.C.; Dhar, A.; Gupta, A.K. *Mater. Sci. Eng*. **2001,** A *304*, 587. **PII:** S0921-5093(00)01540-9
26. Cui, C.; Fritsching, U.; Schulz, A.; Li, Q. *Acta Mater*. **2005,** *53*, 2765. **DOI:** 10.1016/j.actamat.2005.02.047
27. Pedersen, T.B.; Hattel, J.H.; Pryds, N.H. in: Proceedings of the 22nd RISØ International Symposium on Materials Science **2001,** 353.
28. Markus, S.; Cui, C.; Fritsching, U. *Mater. Sci. Eng.* **2004,** *A 383*, 166. **DOI:** 10.1016/j.msea.2004.02.046
29. Hattel, J.H.; Pryds, N.H. *Acta mater*. **2004,** *52*, 5275. **DOI:** 10.1016/j.actamat.2004.07.016
30. Pryds, N.H.; Hattel, J.H. *Int. J. Therm. Sci*. **2005,** *44*, 587. **DOI:** 10.1016/j.ijthermalsci.2005.01.001
31. Ward, R.M.; Barratt, M.D.; Jacobs, M.H.; Zhang, Z.; Dowson, A.L. *J. Mater. Sci.* **2004,** *39*, 7259. **DOI:** 10.1023/B:JMSC.0000048740.09872.51
32. Mi, J.; Grant, P.S. *Acta Mater.* **2008,** *56*, 1588. **DOI:**10.1016/j.actamat.2007.12.0210
33. Singh, D.; Dangwal, S. *J. Mater. Sci*. **2006,** *41*, 3853. **DOI:** 10.1007/s10853-006-6652-2
34. Singh, D.; Tomar, A.; Ojha, K.V. *Steel Res. Int.* **2007,** *78*, 241.
35. B. See and G.H. Johnston, *Powder Tech.* **1978,** *21*, 119.
36. Srivastava, V.C.; Mandal, R.K.; Ojha, S.N.; Venkateswarlu, K. *Mater. Sci. Eng.* **2007,** *A 471*, 38. **DOI:**1016/j.msea.2007.04.109
37. Osorio, W.R.; Garcia, L.R.; Goulart, P.R.; Garcia. *Mater. Chem. Phys*. **2007,** *106*, 343. **DOI:** 10.1002/maco.200905420
38. Heiberg, G.; Armberg, L. *J. Light Metals* **2001,** *1*, 43. **PII:** S 1 4 7 1 - 5 3 1 7 (0 0) 0 0 0 0 5 – 5

